The Role of Moist Baroclinic Instability in the Growth and Structure of Monsoon Depressions

J. A. ARAVEQUIA, V. BRAHMANANDA RAO, AND J. P. BONATTI

Instituto Nacional de Pesquisas Espaciais, São José dos Campos, Sao Paulo, Brazil

(Manuscript received 2 November 1994, in final form 24 March 1995)

ABSTRACT

The effect of latent heat of condensation on baroclinic instability process is studied using the model developed by Bonatti and Rao. This model includes the effect of latent heat of condensation as parameterized by Mak, a zonal wind profile that varies linearly with pressure, and a constant lapse rate of $-6°C\ km^{-1}$. The effect of dissipative terms and vertical variation of heating on baroclinic instability with positive and negative zonal wind shears is studied.

Dissipative terms and the type and intensity of heating change the selection of the most unstable wave. Viscosity and Newtonian cooling stabilize short waves. The characteristics of the most unstable wave obtained using a double maximum in the vertical distribution of heating and observed vertical profiles of zonal wind and temperature representative of the summer monsoon of India resemble those of observed monsoon depressions. The inclusion of dissipative effects makes the Green mode the most unstable wave.

1. Introduction

During the summer monsoon season, India and its neighboring area are characterized by an easterly zonal wind shear with low-level westerlies decreasing with height and culminating in an easterly jet in the upper troposphere. Among several disturbances which form in this region, monsoon depressions (MDs) (Saha and Chang 1983) are responsible for copious amounts of rainfall over India. They form over the north Bay of Bengal and move westward to northwestward. Many of these disturbances seem to possess a cold core in the lower levels and a warm core aloft (Krishnamurti et al. 1976; Godbole 1977; Saha and Chang 1983), although different thermal structures have also been observed (Nitta and Masuda 1981). These disturbances have a horizontal scale of around 3000 km and a westward phase velocity of about $3\ m\ s^{-1}$.

The mechanism for generation of MDs has been the subject of investigation by many authors (Shukla 1977, 1978; Satyan et al. 1980; Mishra and Salvekar 1980; Moorthi and Arakawa 1985 and others). Some of these authors considered the baroclinic instability of the zonal wind with easterly shear. Shukla (1978) studied the combined conditional instability of the second kind, barotropic, and baroclinic instability of the observed monsoon zonal flow and stressed the importance of cumulus heating for the development of MDs. Moorthi and Arakawa (1985) made a thorough investigation of how cumulus heating affects baroclinic instability of zonal flows with westerly and easterly shears. They used two formulations of cumulus heating, one in which heating at all levels is proportional to the vertical velocity at the top of the lowest layer and the other following Arakawa and Schubert (1974). Moorthi and Arakawa (1985) found that the Green modes are destabilized by cumulus heating for easterly shears. They interpreted MDs as the Green mode since this is the only mode with westward phase speed similar to the observed MDs. The geopotential height structure of this mode showed little tilt up to 500 hPa, above which it tilted eastward. The thermal anomalies also showed an eastward tilt.

Recently Douglas (1992a,b) discussed in detail the structure and dynamics of two monsoon depressions observed during the 1979 Summer Monsoon Experiment. One important difference between the observed structure and the structure of the wave that Moorthi and Arakawa (1985) associated with MDs is the vertical structure of the temperature anomalies. In contrast to Moorthi and Arakawa's (1985) theoretical disturbance's eastward tilt, Douglas (1992a) observed a westward tilt. However, Moorthi and Arakawa's (1985) theoretical disturbance showed a cold core in the lower troposphere and a warm core in the upper troposphere, as in the case of the observed monsoon depressions.

The purpose of the present study is to extend Moorthi and Arakawa's (1985) analysis, considering the effect of double maxima in the heating profile on moist baro-

Corresponding author address: Dr. V. B. Rao, Instituto Nacional de Pesquisas Espaciais, CP 515, 12201-970 Sao José dos Campos, Sao Paulo, Brazil.

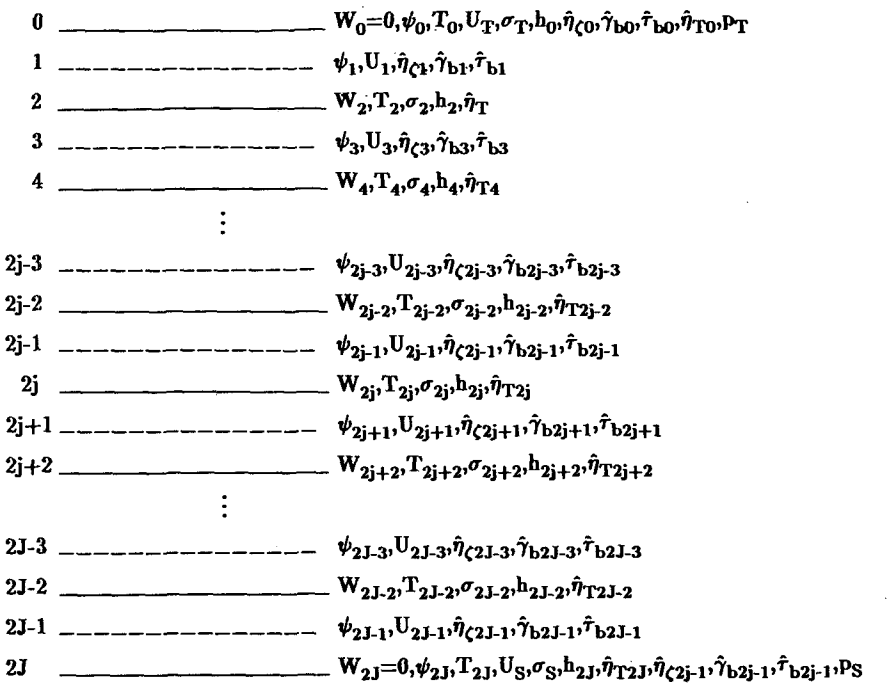

FIG. 1. Vertical grid of variables for J layers.

clinic instability. Douglas (1992a) obtained a zonal and a vertical section of temperature anomaly in the case of two observed monsoon depressions. His Fig. 13 suggests the existence of two maxima, one in the lower levels (around 900 hPa) and the other the between 500- and 300-hPa levels. Recent study of Lupo et al. (1992) shows the vertical variation of latent heat release for two intense cyclones. Although their study is for a different region, their Fig. 29 also shows that latent heating can have two maxima, one in the lower levels and the other in the upper levels. In the present study we also investigate the role of cumulus friction, as formulated by Schneider and Lindzen (1976), and dissipation on moist baroclinic instability. In the case of monsoon depressions Daggupaty and Sikka (1977) pointed out that cumulus friction is important in the vorticity budget. Wang et al. (1985) studied the effect of Newtonian cooling and Ekman dissipation on the dry baroclinic instability. Their results showed that the midlatitude planetary waves 2–4 belong to the intermediate-scale motion between the Charney and Burger modes and may be viewed as the most unstable Green mode. They also noted that Newtonian cooling can have a destabilizing effect. Wang (1990) examined the asymmetry of baroclinic instability between easterly and westerly shear, again for a dry atmosphere. Thus, the present study extends the analysis of Wang et al. (1985) and Wang (1990) by considering latent heating for both westerly and easterly shears. We use Mak's (1982) parameterization of latent heating as discussed earlier by Bonatti and Rao (1987).

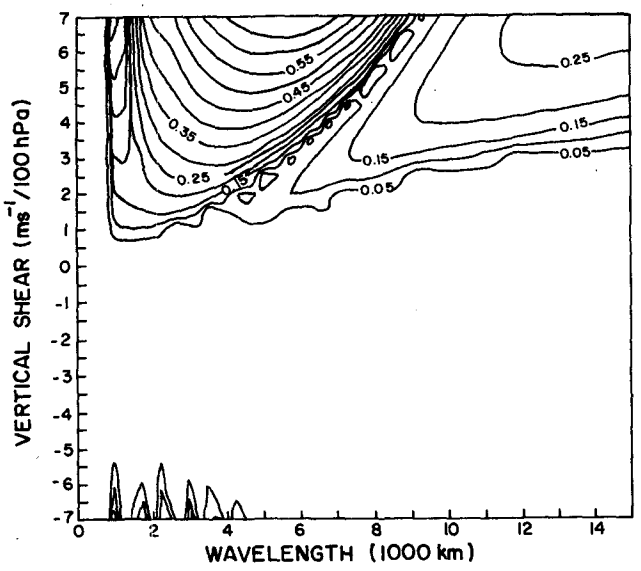

FIG. 2. Growth rates (in day^{-1}) as functions of wavelength and vertical shear obtained from the 18-level model without heating and dissipative effects.

In a recent study using elegant mathematical analysis Mak (1994) generalized the heating parameterization. However, his previous parameterization (Mak 1982) is still a good approximation of the general result when

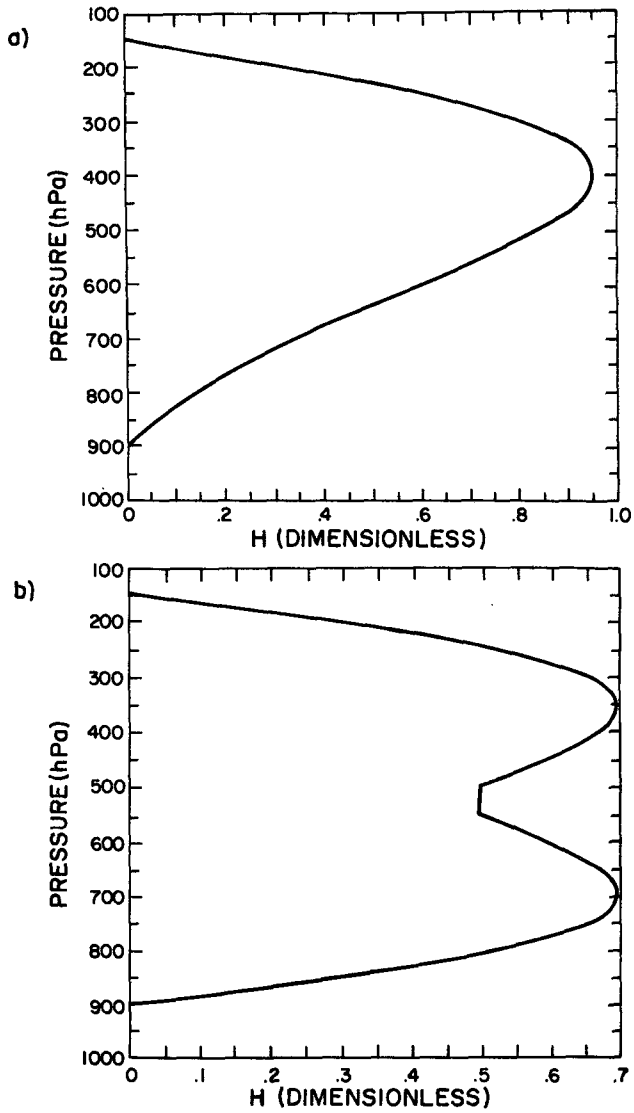

FIG. 3. Vertical structure of heating function for (a) one maximum and (b) two maxima.

the heating intensity is relatively weak. The monsoon depression case, unlike that of violent disturbances such as the *Queen Elizabeth II* (*QE-II*) storm over the ocean (Kuo et al. 1991), may probably be considered as the weak heating case. Observed pressure deepening in the *QE-II* storm could be as much as 59 mb in 24 h, while in the monsoon disturbances studied by Douglas (1992a) the pressure drop was around 18 mb in 7 days for the onset vortex and 6 mb in 4 days for the July depression (Figs. 3 and 16).

2. The model equations

The model equations and methodology used to solve them have already been given in Bonatti (1987), Bonatti and Rao (1987), and Aravequia (1993). Here we briefly discuss the method giving emphasis to the description of the terms that were not included in the model given by Bonatti and Rao (1987).

The basic equations of the model are the vorticity and thermodynamic energy equation given, respectively, as

$$\frac{\partial \xi}{\partial t} + \mathbf{V}_g \cdot \nabla(\xi_g + f) = f_0 \frac{\partial \omega}{\partial p} - \frac{\partial}{\partial p}[M_c(\xi_g - \xi_{gc})] - \eta_\xi \xi_g \quad (1)$$

$$\frac{\partial}{\partial t}\left(\frac{\partial \phi}{\partial p}\right) + \mathbf{V}_g \cdot \nabla\left(\frac{\partial \phi}{\partial p}\right) + \sigma\omega = -\frac{R\dot{Q}}{Pc_p} - \eta_T\left(\frac{\partial \phi}{\partial p}\right), \quad (2)$$

where $\xi_g = \nabla^2\phi/f_0 = \nabla^2\psi$ is the geostrophic vorticity; $\xi_{gc} = \nabla^2\phi_c/f_0 = \nabla^2\psi_c$ is the geostrophic vorticity at a level of finite-difference model nearest to the base of the cloud; $M_c = M_{c0}\nu(p)$ is the upward mass flux; M_{c0} is the upward mass flux at a level of finite-difference model nearest to the base of cloud; $gM_{c0} = 6.94 \times 10^{-4}$ hPa s^{-1}, the same value as used by Geisler (1981); $\eta_\xi = \eta_\xi(p)$ is the Rayleigh-type of frictional coefficient (s^{-1}); $\eta_T = \eta_T(p)$ is the coefficient of Newtonian cooling (K s^{-1}); $\nu(p) = 1 - \exp[-(p - p_{TN})/p_d]$; $p_{TN} = 140$ hPa and $p_d = 100$ hPa; $\eta_\xi(p) = 1.1574 \times 10^{-6} \exp[(p - 1000)/200]$; $\eta_T(p) = 2.315 \times 10^{-6} + 4.052 \times 10^{-6} \exp(2.636p^*) \sin(\pi p^*)$; and $p^* = p - 100/900$.

For a list of symbols see the appendix.

The Rayleigh-type friction will have its maximum value at the surface with a e-folding dissipation of 10 days. The Newtonian cooling is maximum at 750 mb and is adjusted according to Hess's (1959) Fig. 10.4.

The heating parameterization used here was originally proposed by Mak (1982). It is done considering that the heating is proportional to the vertical velocity (ω) induced baroclinically at the base of the cloud, which is given here as P_b. The heating is given by

$$\dot{Q}(x, y, p, t) = -\epsilon c_p h(p) \hat{\omega}_a(x, y, P_b, t),$$

where ϵ (K hPa^{-1}) is an arbitrary constant related to the intensity of heating, $h(p)$ is a function that gives the vertical structure of latent heat of condensation, and $\hat{\omega}_a$ is the adiabatic part of the vertical velocity (ω). For further details see Mak (1982) and Bonatti and Rao (1987).

It should be mentioned here that M_c given above is the zonally averaged cumulus mass flux. The value of 6.94×10^{-4} hpa s^{-1} adopted here corresponds to a zonal average rainfall of 2.2 m. Since this precipitation is distinct from the zero-zonal-average precipitation

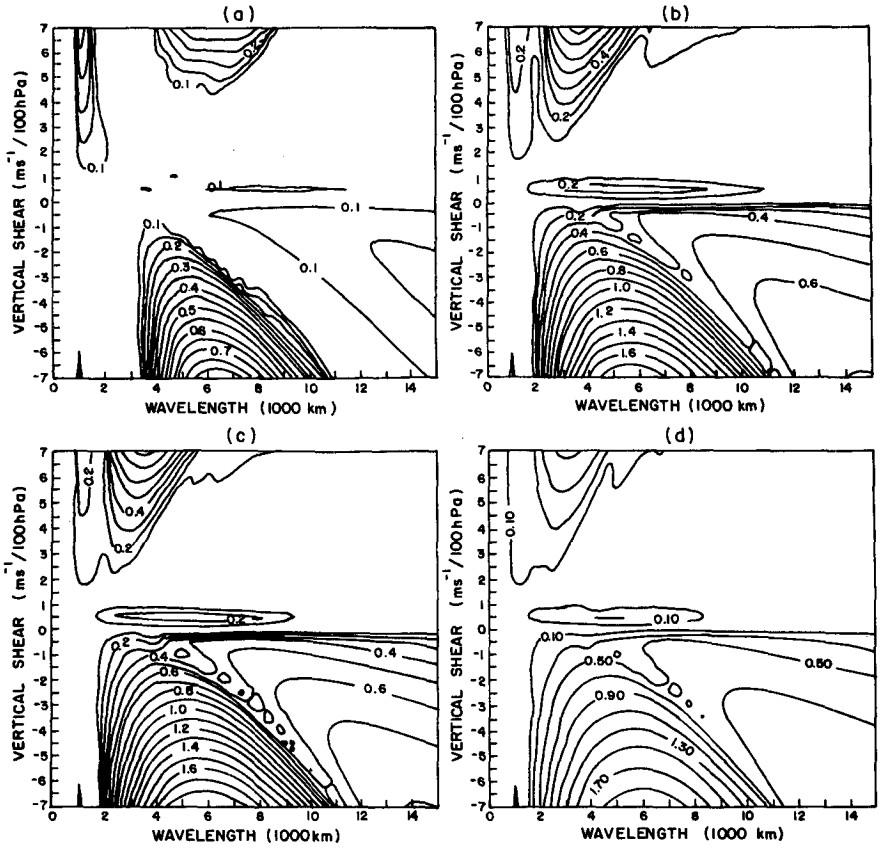

FIG. 4. As in Fig. 2 but with heating having one maximum in the vertical. (a) $\epsilon = 0.2$ K hPa^{-1}, (b) $\epsilon = 0.6$ K hPa^{-1}, (c) $\epsilon = 0.7$ K hPa^{-1}, (d) $\epsilon = 0.8$ K hPa^{-1}.

pattern that produces the model heating function $\dot{Q}$, it is not necessary to relate the vertical profile of M_c to the vertical profile of $\dot{Q}$. For further details see Geisler (1981).

A normal-mode finite-difference multilevel model is developed and is similar to that given by Bonatti and Rao (1987) except that in the present case dissipation terms and cumulus friction are added as given in Eqs. (1) and (2). The vertical grid is given in Fig. 1. The vorticity equation is applied at odd levels, and the thermodynamic energy equation at even levels. The vertical boundary conditions are vanishing vertical p-velocities (ω) at the bottom (p_s) and at the top (p_t) levels. The vertical grid used is a natural extension of the Phillips (1954) grid and thus will not produce spurious modes as pointed out by Arakawa and Moorthi (1988).

3. Energetics

The energy relationships can be obtained from the vorticity equation and from the thermodynamic energy equation. They are given by

$$\frac{dK}{dt} = C(P', K) + D\eta_\xi + DK_b \tag{3}$$

$$\frac{dP'}{dt} = C(\bar{P}, P') - C(P', K) + G + D\eta_T, \tag{4}$$

where K is the eddy kinetic energy, P' the eddy available potential energy, $\bar{P}$ the basic-state available potential energy, G the generation of P' by the heating term, and $C(A, B)$ means the conversion from A to B, if positive. The terms in Eqs. (3) and (4) are volume-integrated quantities in an (x, y, p) system over one wavelength and are given by

$$K = \frac{1}{2}\left\langle \left(\frac{\partial \psi'}{\partial x}\right)^2 + \left(\frac{\partial \psi'}{\partial y}\right)^2 \right\rangle, \tag{5}$$

$$P' = \frac{f_0}{2}\left\langle \frac{1}{\sigma}\left(\frac{\partial \psi'}{\partial p}\right)^2 \right\rangle, \tag{6}$$

$$C(P', K) = f_0\left\langle \omega' \frac{\partial \psi'}{\partial p} \right\rangle, \tag{7}$$

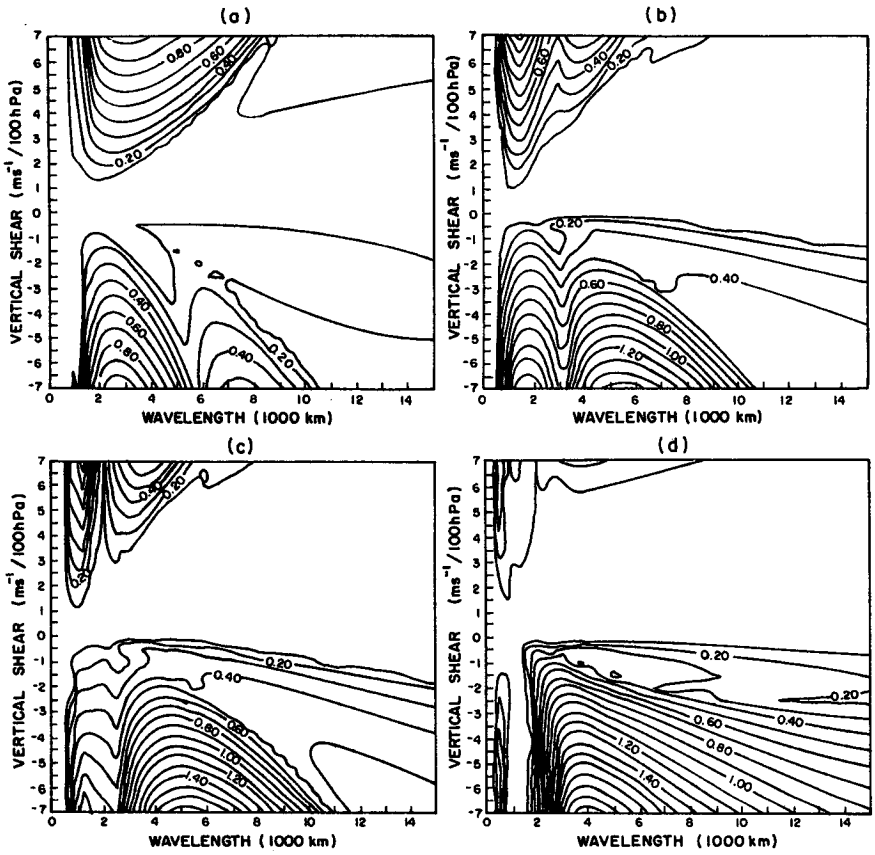

FIG. 5. As in Fig. 5 but with heating having two maxima in the vertical.

$$C(\bar{P}, P') = f_0^2 \left\langle \frac{1}{\sigma} \frac{dU}{dp} \frac{\partial \psi'}{\partial x} \frac{\partial \psi'}{\partial p} \right\rangle, \tag{8}$$

$$G = -\frac{Rf_0}{c_p} \left\langle \frac{\dot{Q}'}{p\sigma} \frac{\partial \psi'}{\partial p} \right\rangle, \tag{9}$$

$$D_{\eta_\xi} = \langle \eta_\xi \psi' \nabla^2 \psi' \rangle, \tag{10}$$

$$D_{\eta_T} = \left\langle -\eta_T \frac{f_0^2}{\sigma} \left(\frac{\partial \psi'}{\partial p} \right)^2 \right\rangle, \tag{11}$$

$$DK_b = \langle K_d \psi' \nabla^2 (\psi' - \psi_b') \rangle + \left\langle K_b \psi' \nabla^2 \left(\frac{\partial \psi'}{\partial p} \right) \right\rangle, \tag{12}$$

$$K_b = gM_c, \tag{13}$$

and

$$K_d = g \frac{dM_c}{dp}, \tag{14}$$

where

$$\langle\langle \quad \rangle\rangle = \left[\frac{1}{2LD(p_s - p_T)} \int_{p_T}^{p_s} \int_{-D}^{D} \int_0^L (\quad) dx dy dp \right]. \tag{15}$$

Note that in the expression for K an additional term (the second term) appears. This is due to the fact that perturbations are assumed to also be functions of the y coordinate $\langle$e.g., $\psi'(x, y, p, t) = \mathrm{Re}\{\hat{\psi} \exp[ik(x - ct)] \sin[l(y - y_0)]\}\rangle$. Also note that the conversion between the eddy kinetic energy and basic-state kinetic energy is not included, since the basic-state zonal wind U is not a function of y.

4. Results and discussion

In this section we present results of the moist baroclinic instability model described in section 2. Experiments are conducted with and without frictional effects and varying the intensity and shape of latent heating. We used an 18-layer model with 100 hPa as the highest level and 1000 hPa as the lowest level. We assume that the basic zonal flow U is a linear function of pressure

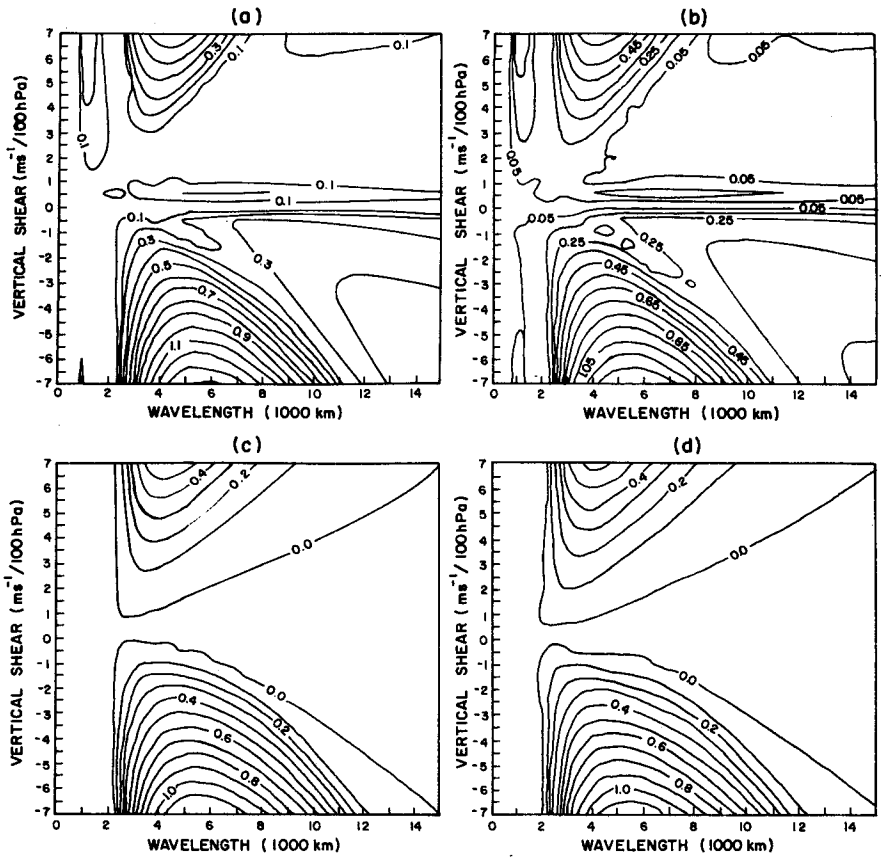

FIG. 6. As in Fig. 2 but with heating having one maximum in the vertical: $\epsilon = 0.4$ K hPa^{-1}. (a) Without dissipative effects, (b) with cumulus friction, (c) with Rayleigh friction and Newtonian cooling, (d) with all the effects.

except in section 4c, and the temperature lapse rate is -6.0°C km^{-1}. This value of the temperature lapse rate is a fairly good representative of the tropical atmosphere and maintains asymmetry of baroclinic instability between easterly and westerly shears (Moorthi and Arakawa 1985).

a. *Results with constant wind shear without frictional effects*

Figure 2 shows the growth rates of baroclinic instability without heating and frictional effects. For westerly shears one can note Charney modes for relatively shorter wavelengths and Green modes for longer wavelengths. For easterly shears baroclinic instability occurs only for high wind shears. These results are similar to those obtained by Moorthi and Arakawa (1985). Wang (1990) using a continuous adiabatic model also noted asymmetry of baroclinic instability between easterly and westerly shears. However, Wang (1990) found some differences between continuous and finite-difference models. He did not find a shortwave cutoff in the continuous model. This difference he attributed to the lack of resolution in a multilevel model. Although in both continuous and finite-difference models a long-wave cutoff exists, there are quantitative differences. For a recent discussion of the shortwave cutoff in a classic Eady (1949) problem and its relevance to the atmosphere see Lindzen (1993, 1994).

The vertical structure for a wavelength of 1112 km and for a shear of 4 m s^{-1} (100 hPa)$^{-1}$ (not shown here) shows that the maximum amplitude is confined to lower levels. This can be identified as the Charney mode. The vertical structure for a wavelength of 9900 km shows (not shown here) that the wave has a large vertical extension and can be identified as the Green mode. These results are similar to those shown by Moorthi and Arakawa (1985) and others.

To verify the effect of including latent heating, we use two types of heating profiles, as shown in Fig. 3. It can be seen that in Fig. 3a one maximum in heating is located around 400 hPa and that in Fig. 3b there are two maxima, one around 350 hPa and the other around 700 hPa. Growth rates of baroclinic instability are ob-

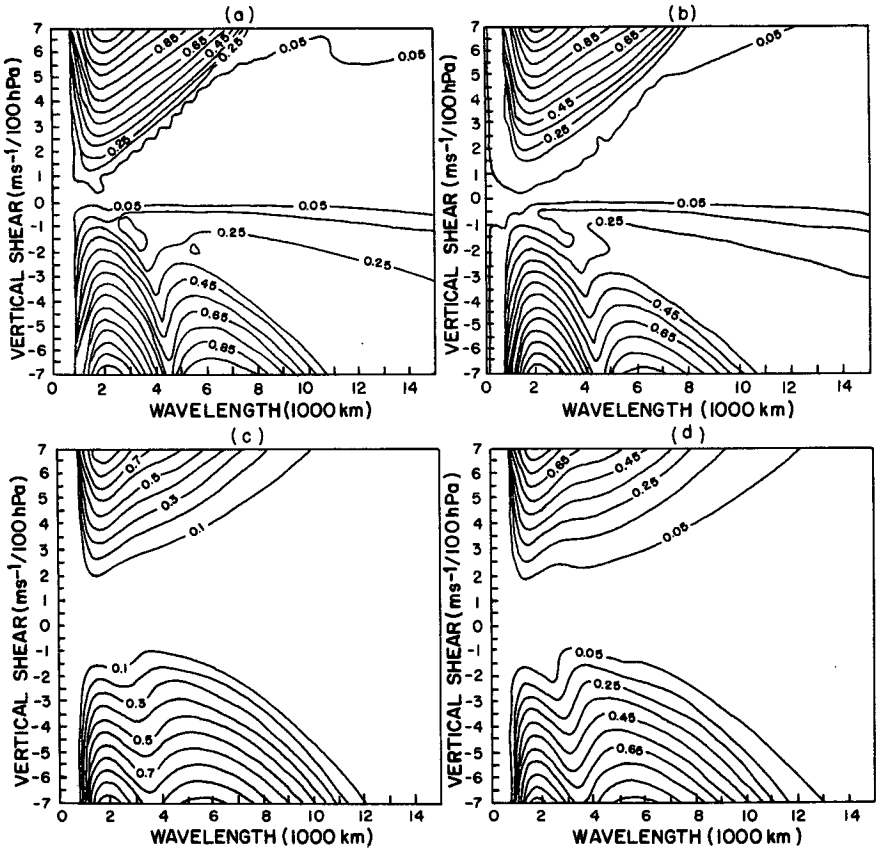

FIG. 7. As in Fig. 6 but with heating having two maxima.

tained for different intensities of latent heating as given by the parameter ϵ.

Figure 4 shows the growth rates of baroclinic instability with latent heating having one maximum around 400 hPa as shown in Fig. 3a. Very few unstable waves are seen for strong easterly shears around 1000 km. At higher wavelengths there is a large unstable region. As the intensity of latent heating increases, the lowest wavelength of this unstable region decreases. For positive shears, for a low heating rate $\epsilon = 0.2$ K hPa^{-1} (Fig. 4a), the Charney modes between 1000 and 2000 km can be seen, and these are separated from the Green modes between 4000 and 9000 km. As the intensity of latent heating increases, both the Charney and Green modes are stabilized for positive shears. Comparing Figs. 2 and 4, one can note that the effect of including latent heating is to stabilize the Charney and Green modes for positive shears and destabilize the Green modes for negative shears. These results agree with those reported by Moorthi and Arakawa (1985).

Figure 5 shows the growth rates of baroclinic instability with latent heating having two maxima in the vertical, as shown in Fig. 3b. For negative shears and low heating rate (Fig. 5a) one can note two regions of instability, one with a most unstable wavelength around 3000 km and the other with a most unstable wavelength around 7000 km. These two modes can be identified as the Charney and Green modes, respectively. As the heating rate increases, the Charney modes become stabilized, and the Green modes become more and more dominant.

Moorthi and Arakawa (1985) interpreted the stabilization of the Charney mode for higher heating rates (η) in terms of the vertical variation ω amplitude for increasing values of latent heating. Based on these values, they concluded that for large values of η the steering level or critical level (the level at which the basic flow U is equal to the phase velocity of the wave c) does not have significant geopotential amplitude, leading to stabilization. They also suggested that for the Green modes the destabilization is due to the occurence of reasonable values of geopotential amplitudes at the steering levels. The role of critical levels in baroclinic instability was discussed by Bretherton (1966).

Comparison of Figs. 4 and 5 shows that the effect of double maxima in the heating rate favors the growth of the Charney modes for positive shears and for low heating rates. For negative shears the Green modes become

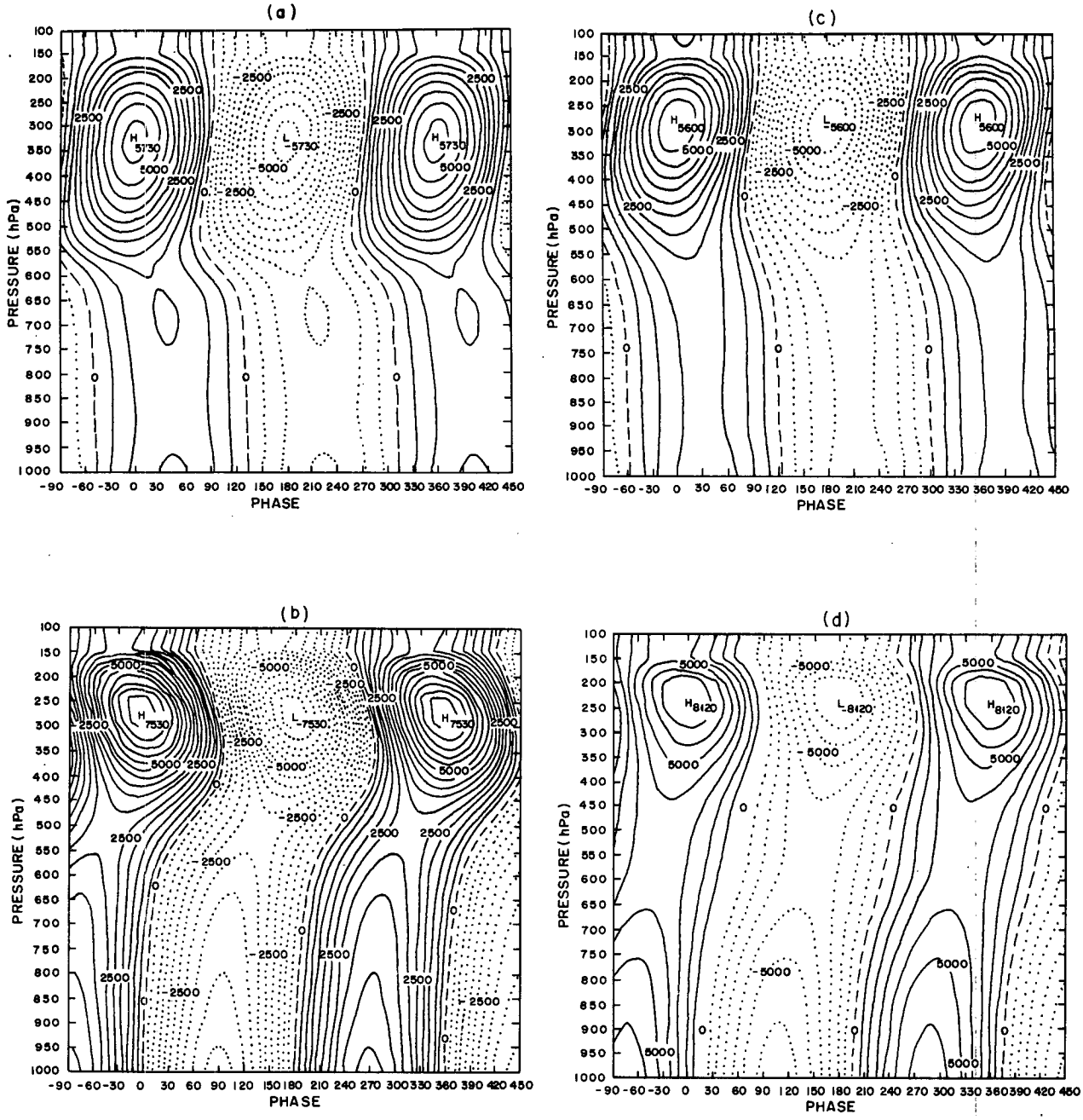

FIG. 8. Pressure–longitude cross section of streamfunction in $m^2 s^{-1}$ of the most unstable modes with one maximum in heating (a) with cumulus friction, zonal wind shear of 4 m s^{-1} (100 hPa)$^{-1}$, and a wavelength of 3600 km, (b) with cumulus friction, zonal wind shear of −4 m s^{-1} (100 hPa)$^{-1}$, and a wavelength of 4925 km, (c) with Rayleigh friction and Newtonian cooling, zonal wind shear of 4 m s^{-1} (100 hPa)$^{-1}$ and a wavelength of 3775 km, (d) with Rayleigh friction and Newtonian cooling, zonal wind shear of −4 m s^{-1} (100 hPa)$^{-1}$, and a wavelength of 5150 km, (e) with all the dissipative effects, zonal wind shear of 4 m s^{-1} (100 hPa)$^{-1}$, and a wavelength of 3625 km, (f) with all the dissipative effects, zonal wind shear −4 m s^{-1} (100 hPa)$^{-1}$, and a wavelength of 4875 km.

more dominant. One can note unstable Charney modes in the double-heating profile that are stable in the single maximum heating case. Heating in the lower levels (700 hPa) probably favors growth of the Charney modes, which are confined to lower levels.

b. Results with constant wind shear and dissipative effects

Figs. 6 and 7 show the growth rates of baroclinic instability when the dissipative effects are included.

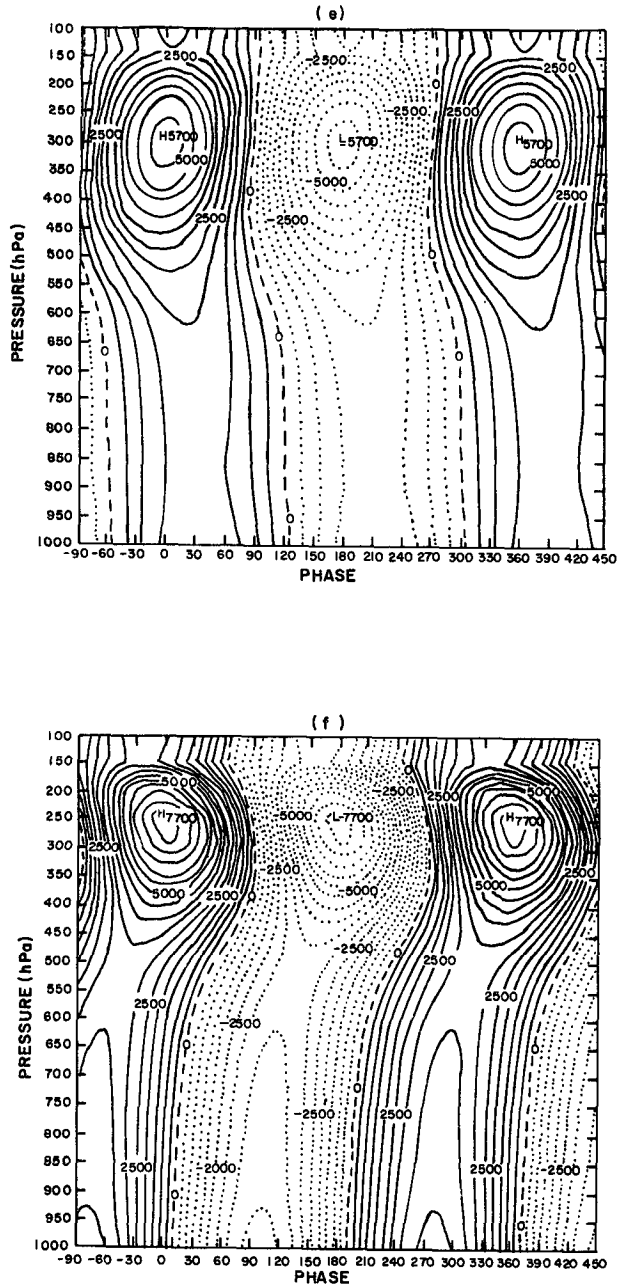

FIG. 8. (*Continued*)

Figure 6 shows the case of a single maximum in the heating profile, and Fig. 7 shows the case of double maxima in the heating profile. It can be seen in Fig. 6 that for both easterly and westerly shears the wavelength of the most unstable wave increases with shear. A similar feature is noted by Wang et al. (1985) and others for the westerly shear case in a dry atmosphere. In Figs. 6 and 7 one can note that the inclusion of all the three dissipative effects, namely, cumulus friction, Rayleigh friction, and Newtonian cooling, in general stabilizes all the modes for easterly shears. A comparison of Figs. 6 and 7 shows that some waves shorter than 2000 km are destabilized in the case of double maxima in the heating profile. A similar feature is noted earlier in Figs. 4 and 5. Thus, this feature is preserved even in the presence of frictional effects. Figure 7 shows, as expected, that the inclusion of Rayleigh friction and Newtonian cooling reduces the growth rates for shorter waves more than for longer waves, this being particularly true for negative shears. In Fig. 7 one can see that when Rayleigh friction and Newtonian cooling are included the most unstable wave shifts to higher wavelengths in the case of negative shears (cf. Figs. 7a and 7d). On the other hand, the effect of cumulus friction alone does not alter the most unstable wave at 2000 km (cf. Figs. 7a and 7b). Thus, the inclusion of Rayleigh friction and Newtonian cooling effects alters the selection of the most unstable wave favoring the longer waves (Green modes). Analyzing the effect of Ekman dissipation and Newtonian cooling, Wang et al. (1985) noted that Newtonian cooling is more important for the Green mode than for the Charney mode. They found that the separation of the Charney mode and the Green mode becomes less sharp in the presence of Newtonian cooling. A similar effect is noted in Fig. 7 comparing Figs. 7a and 7c. [Also compare Fig. 7 with Fig. 7 of Wang et al. (1985).]

Figures 8 and 9 show the vertical structure of the streamfunction of the most unstable waves given in Figs. 6 and 7 for various combinations of frictional effects. The general structure of Fig. 8 is similar for all the cases, except that, for positive shear the inclination of the trough (or ridge) axis is toward west with height below 300 hPa and for negative shear the inclination is toward east. The maximum amplitude of the streamfunction is located in the upper troposphere for all cases. These can be identified as the Green modes. Note that for negative shears there is a secondary maximum in the lower levels. As is well-known, westward (eastward) inclination indicates poleward (equatorward) heat transport by eddies, thus, converting mean available potential energy into perturbation available potential energy for westerly (easterly) shears.

Figure 9 shows the vertical structure for three unstable modes for the case of a double maximum in the heating profile, without dissipative effects. Figure 9a shows the structure of an unstable wave in the first region of instability with -4 m s^{-1} (100 hPa)$^{-1}$ (Fig. 7a). This mode has a wavelength of 2050 km and has a phase velocity of -17.4 m s^{-1}. This mode shows vertical extension although it is a shortwave. This is due to the second maximum of 350 hPa in the heating profile. However, the higher values are confined to lower levels. This can be identified as the Charney mode destabilized by cumulus heating for negative shears. Figure 9b shows the structure of a mode with a

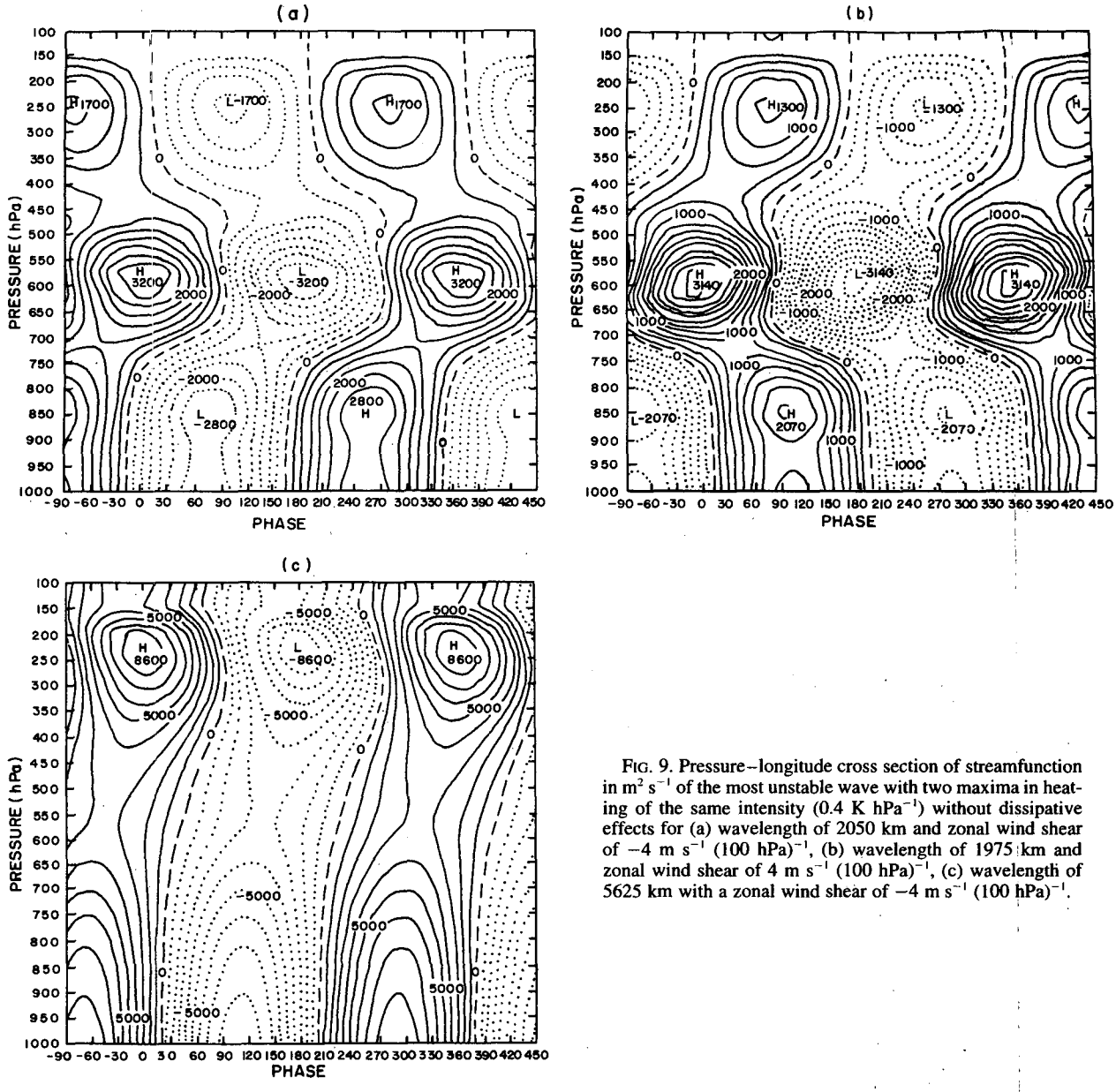

FIG. 9. Pressure–longitude cross section of streamfunction in $m^2 s^{-1}$ of the most unstable wave with two maxima in heating of the same intensity (0.4 K hPa^{-1}) without dissipative effects for (a) wavelength of 2050 km and zonal wind shear of -4 m s^{-1} (100 hPa)$^{-1}$, (b) wavelength of 1975 km and zonal wind shear of 4 m s^{-1} (100 hPa)$^{-1}$, (c) wavelength of 5625 km with a zonal wind shear of -4 m s^{-1} (100 hPa)$^{-1}$.

shear of $+4$ m s^{-1} (100 hPa)$^{-1}$. This mode has a wavelength of 1975 km and a phase velocity of $+15$ m s^{-1}. The vertical structure of this mode is similar to that of Fig. 9a, except that, the inclinations are reversed. At the lower levels the first mode (Fig. 9a) shows an eastward inclination, and the second mode (Fig. 9b) a westward inclination. This indicates a conversion of mean available potential energy into perturbation available potential energy. Although the inclinations are reversed at the higher levels, their contribution for energetics is small because the amplitude is small at these levels. This opposite inclination at higher levels is expected because the negative contribution to vorticity, due to divergence in front of the trough, should be overcompensated for by positive vorticity advection, which makes the upper-level trough remain approximately in phase with the lower-level trough (Moorthi and Arakawa 1985).

Figure 9c shows the structure of the mode with a wavelength of 5625 km and a phase velocity of -31 m s^{-1}. This mode is in the second region of instability for negative shears (Fig. 7a). The streamfunction shows a large vertical extension, and the principal maximum can be located in the upper troposphere. It has

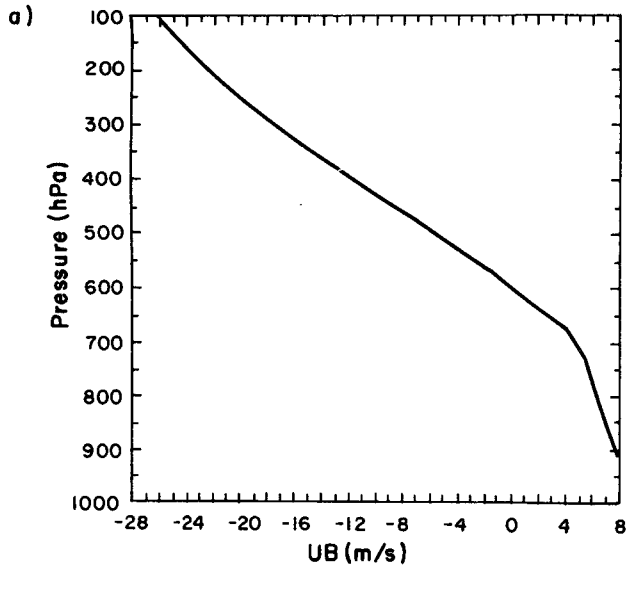

FIG. 10. (a) Zonal wind in m s^{-1} and (b) temperature K for the monsoon case.

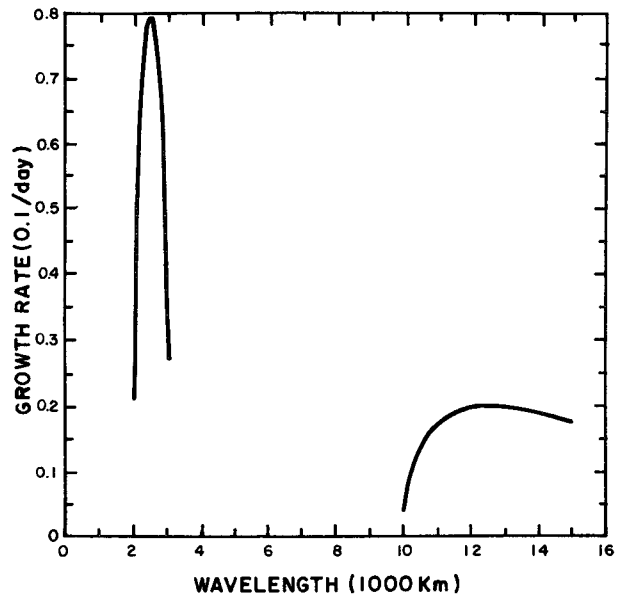

FIG. 11. Growth rates as functions of wavelength in 10^{-1} $days^{-1}$ for the monsoon case without heating and dissipative effects.

an easterly inclination with height showing a conversion of mean available potential energy into perturbation available potential energy. This mode can be identified as the Green mode.

From Figs. 8 and 9 it can be concluded that the inclusion of dissipative effects does not change the vertical structure of the modes. In other words, if a wave is Charney or Green mode without dissipative effects, it continues to be so even in the presence of dissipative effects. However, as noted earlier, inclusion of dissipation effects can affect growth rate such that the most unstable wave for negative shears can be the Green mode.

c. *Application to the Indian monsoon region*

In this section we present results of a study of the linear model applied to the Indian monsoon region. The zonal wind profile is taken from Fig. 15 of Moorthi and

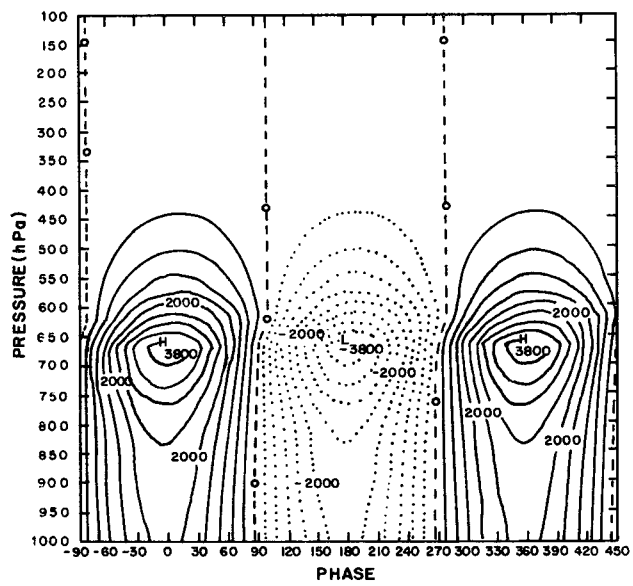

FIG. 12. Pressure–longitude cross section of the streamfunction (in m^2 s^{-1}) for the most unstable wave at 2450 km.

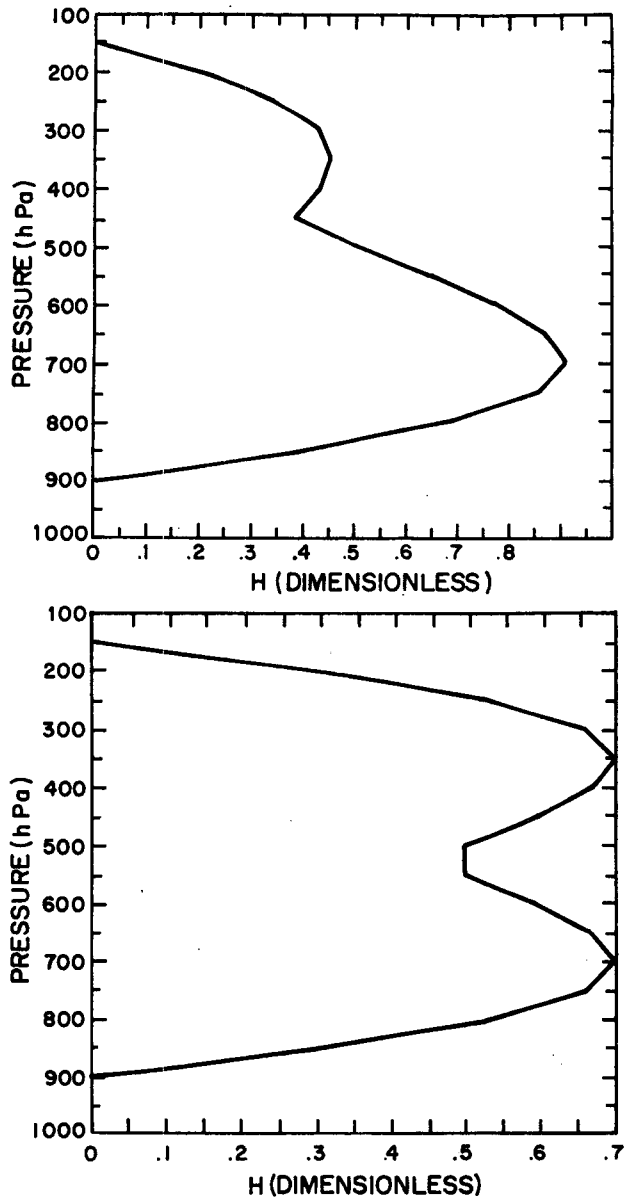

FIG. 13. Vertical profile of heating with $\epsilon = 0.8$ K hPa^{-1} (a) and $\epsilon = 1.6$ K hPa^{-1} (b).

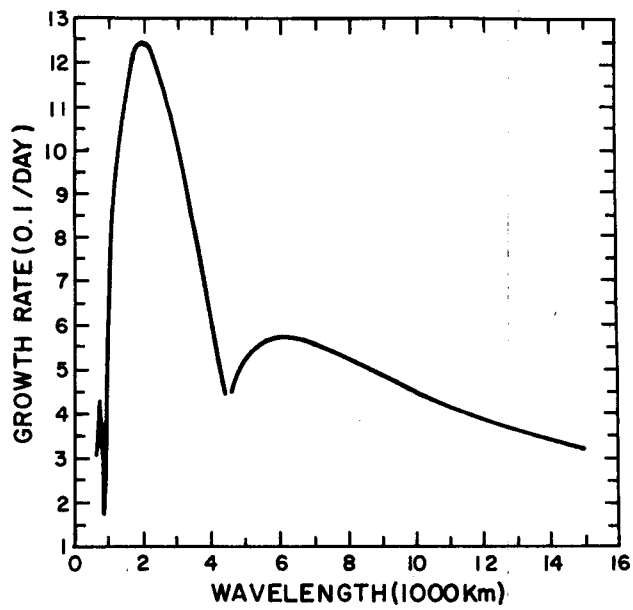

FIG. 14. Growth rates as functions of wavelength for experiment 8 as given in Table 1.

Arakawa (1985) (strong shear case), and the temperature profile is taken from Misra and Salvekar (1980). These are shown in Fig. 10. The value of f taken here is for the latitude 20°N.

In the first experiment heating and dissipative effects are not included. Figure 11 shows the growth rates for this case. In this figure one can note two regions of instability, one narrow region around 2000 km, and the other for more than 10 000 km. The most unstable wave has a wavelength of 2450 km, and the structure of the streamfunction is shown in Fig. 12. This mode is confined to the lower atmosphere and can be identified as the Charney mode. The Green modes appear for wavelengths higher than 10 000 km and have very small growth rates. In order to see the effect of an artificial boundary at 100 hPa, we calculated the growth rates for a 40-level model with the top of the model at 1 hPa. We considered the basic state above 100 hPa as

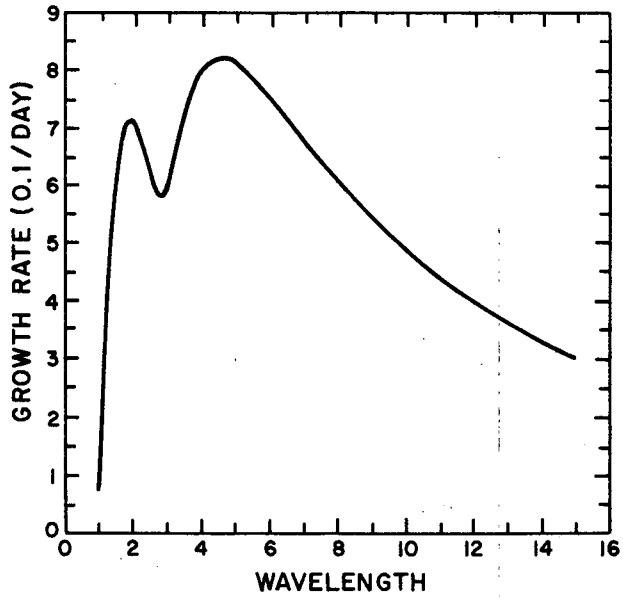

FIG. 15. Growth rates as functions of wavelength for experiment 5 as given in Table 1.

TABLE 1. The most unstable modes for monsoon case.

Expt	Cumulus friction	Rayleigh friction	Newtonian cooling	L (km)	C_r (m s^{-1})	Growth rate (day^{-1})	Group velocity	ϵ (K hPa^{-1})
1	×	×	×	2350	−1.68	0.87	2.5	0.8
2		×	×	2400	−2.53	0.96	2.11	0.8
3	×			2400	−0.76	1.2	−0.4	0.8
4				2400	−1.77	1.3	−0.38	0.8
5	×	×	×	4500	−11.2	0.82	−4.74	1.6
6		×	×	4450	−11.7	0.88	−4.16	1.6
7	×			1950	−1.84	1.1	−1.21	1.6
8				1950	−2.96	1.2	−1.29	1.6
9				2450	+1.4	0.08	3.25	0.0

barotropic and isothermal. We found that the increase of vertical extent has no appreciable influence on the growth rates presented here.

One important difference between the unstable modes in this nonheating case and the observed monsoon depression is the direction movement. The most unstable mode (2450 km) shows positive phase velocity of 1.4 m s^{-1} and positive group velocity of 2.25 m s^{-1}, indicating an eastward movement, while the observed disturbances are known to move westward.

Several experiments are made using two types of heating profiles shown in Fig. 13: in case a, ϵ is taken as 0.8 K hPa^{-1}, and in case b, ϵ is 1.6 K hPa^{-1}. These correspond to the heating rates of 17 K day^{-1} and 24 K day^{-1}, respectively. Although the heating rate of 24 K day^{-1} is somewhat high, note that this heating rate is given at 700 and 350 mb and the vertically averaged heating could be much less than this amount. Table 1 gives the characteristics of the most unstable wave for various combinations of dissipative effects. Table 2 gives the corresponding energetics. It can be seen in Table 2 that the generation of perturbation available potential energy, G, is one order of magnitude greater than the potential energy conversion term $C(\bar{P}, P')$. Also, from Table 1 it can be seen that growth rates of the most unstable waves with heating are one order of magnitude more than the case without heating (experiment 9). This shows that latent heating is essential for the growth of baroclinic modes with easterly shear. Note in Table 2 that the Newtonian cooling is the most intense dissipative affect.

As is well-known [Douglas (1992) and others], monsoon depressions move westward with a phase velocity of about 3–4 m s^{-1}. In Table 1 it can be seen that phase and group velocities are negative (westward propagation) for experiments 3–8. For the experiment with all the effects, 5, the group velocity is −4.7 m s^{-1}.

Figures 14 and 15 show the growth rates as a function of wavelength for experiments 8 and 5. In the case without any dissipative effects, experiment 8, the most unstable wave has a wavelength of 1950 km. However, when all the dissipative effects are included (expt 5), the most unstable wave turns out to be of wavelength 4500 km. A comparison of Fig. 14 and 15 shows that although shortwaves are stabilized by frictional effects the growth rates of waves around 4500 km increased slightly (from 0.55 day^{-1} to 0.82 day^{-1}). At first sight this seems contradictory to what is expected. However, several authors (Chandrasekhar 1961; Holopainen 1961; Yamasaki 1969; Satyamurty 1983) noted that friction can give rise to unexpected destabilization. Satyamurty (1983) discussed the role of friction in the generation of sub-synoptic-scale unstable baroclinic waves. His case 4 corresponds to the Rayleigh friction we used. His Fig. 2 shows the formation of a new region of instability at intermediate scale and, more rel-

TABLE 2. Energetics of the most unstable modes for the monsoon case. The values of K and P are in percent of total energy. The terms $C(\bar{P}, P')$, $C(P', K')$, G, D_{η_ϵ}, D_{η_T}, and DK_h are in 10^{-6} m^2 s^{-3}.

Expt	L km^{-1}	K	P'	$C(\bar{P}, P')$	$C(P', K')$	G	D_{η_ϵ}	D_{η_T}	DK_h
1	2350	74.55	25.45	2.44	16.82	30.08	−0.68	−10.54	−1.15
2	2400	75.96	24.04	2.52	17.53	30.25	−0.68	−9.92	
3	2400	65.24	34.76	1.39	18.7	26.57			−1.29
4	2400	68.02	31.98	1.58	19.81	27.55			
5	4500	77.41	22.59	1.54	16.55	27.36	−0.51	−8.06	−1.34
6	4450	77.64	22.36	1.38	16.44	27.11	−0.48	−7.46	
7	1950	59.74	40.26	0.96	16.07	25.31			−0.92
8	1950	63.4	36.60	1.42	18.34	27.5			
9	2450	73.39	27.61	1.83	1.33				

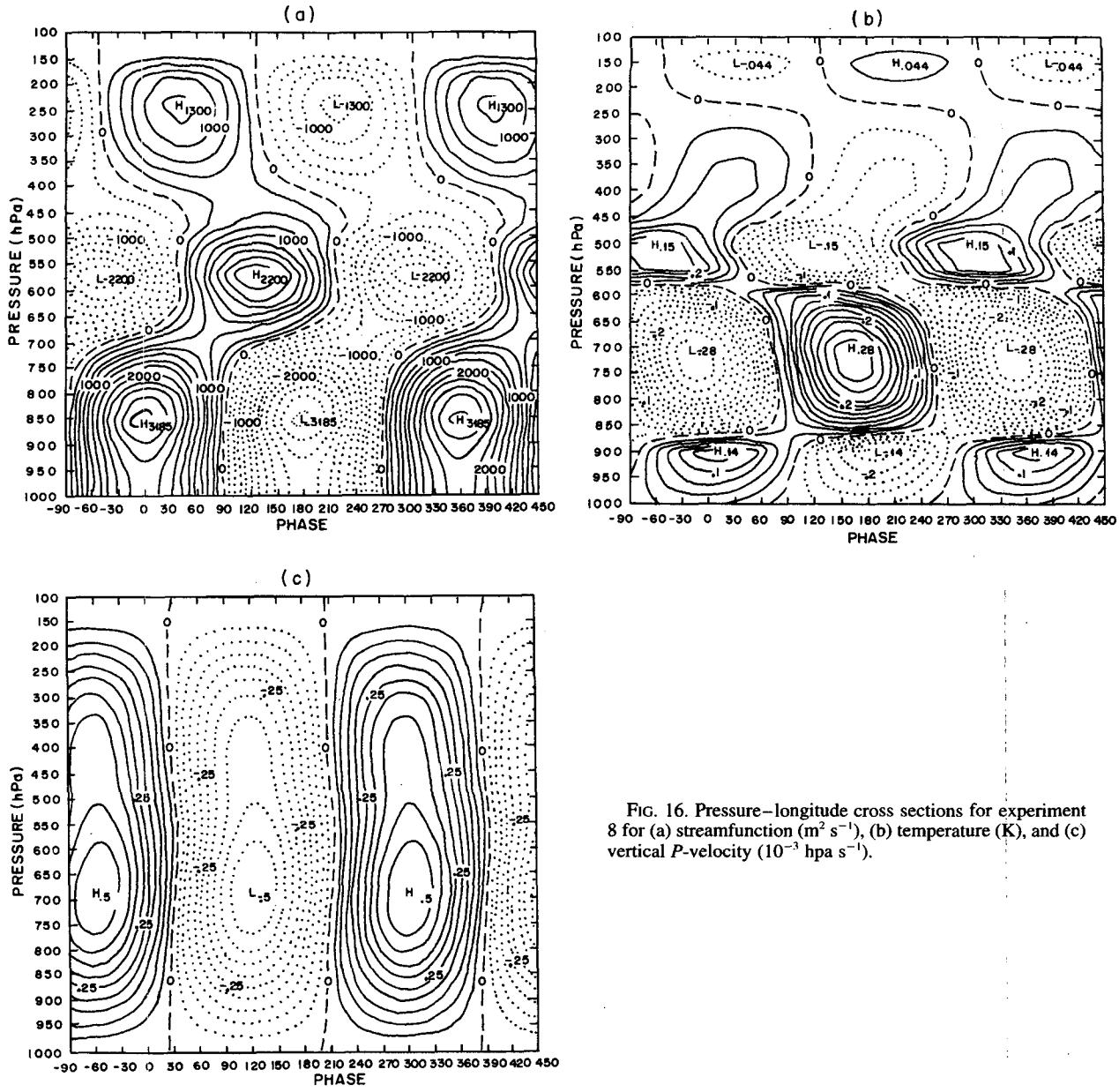

FIG. 16. Pressure–longitude cross sections for experiment 8 for (a) streamfunction ($m^2 s^{-1}$), (b) temperature (K), and (c) vertical P-velocity (10^{-3} hpa s^{-1}).

evantly for the present study, the increase of growth rates (decrease of e-folding time) at longer wavelengths. However, in our study we included additional dissipative effects such as Newtonian cooling and cumulus friction, while Satyamurty used only westerly shears. Thus, some differences are expected, such as the stabilization of shortwaves in our case.

Figures 16 and 17 show the vertical structure of the modes for experiments 5 and 8. The vertical structure of the first mode (wavelength 1950) is similar to that of a Charney mode. Also, note in Fig. 16b a cold core in the lower levels below 850 mb and a warm core in the upper levels with a maximum around 750 mb. In this case the temperature shows a westward inclination in the layer between 800 and 450 hPa, where the principal maximum of streamfunction is concentrated. From the vertical velocity ω and temperature structure (Figs. 16b and 16c), a direct thermal circulation of hot air rising and cold air sinking can be seen between 600 and 950 hPa. This indicates, as is well-known, a conversion of eddy potential energy into eddy kinetic energy.

In Fig. 17a it can be seen that the streamfunction has a large vertical extension similar to that of a Green mode. Also, note in the streamfunction low (pressure)

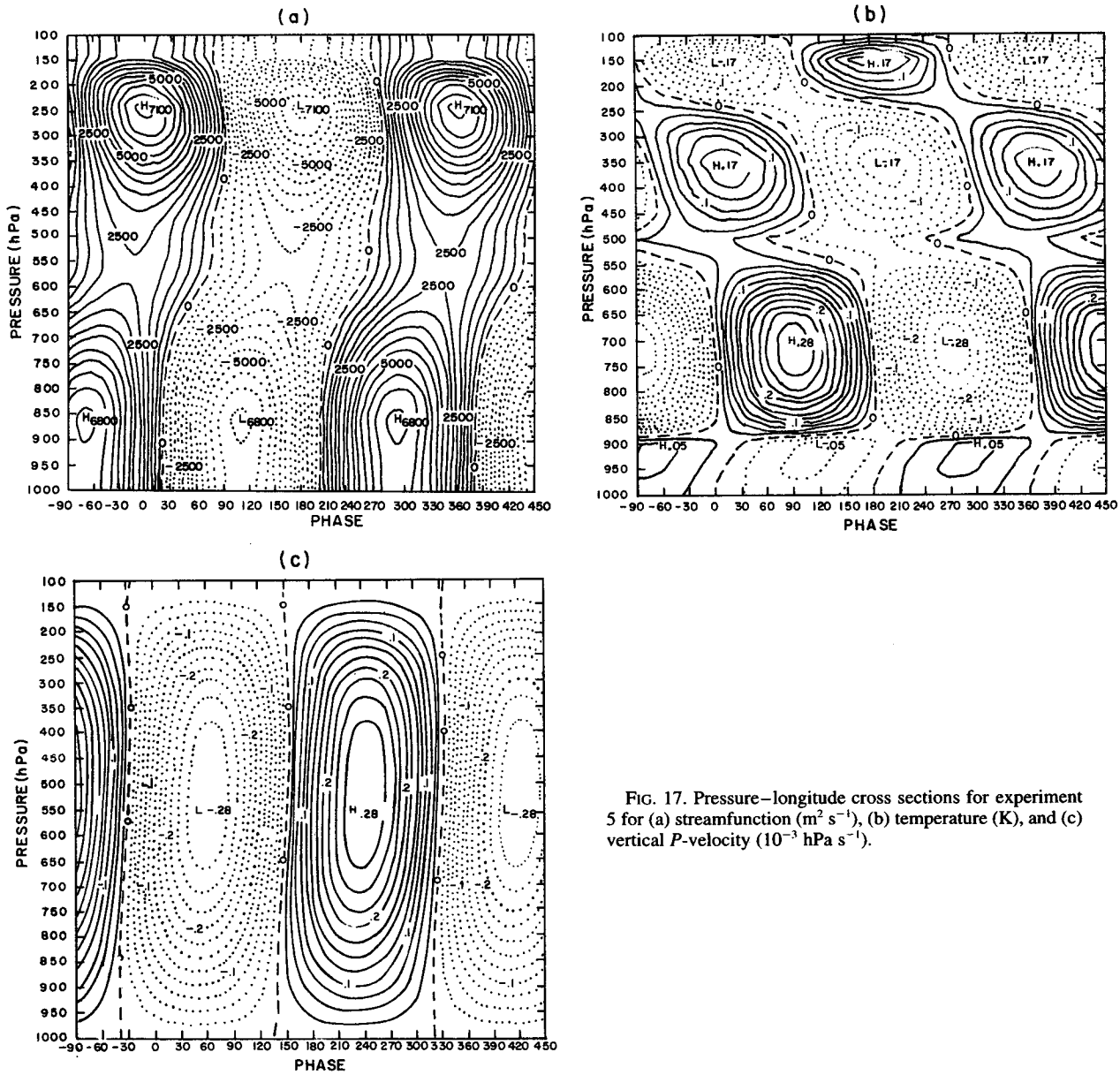

FIG. 17. Pressure–longitude cross sections for experiment 5 for (a) streamfunction ($m^2\ s^{-1}$), (b) temperature (K), and (c) vertical P-velocity (10^{-3} hPa s^{-1}).

center there is a minimum in the lower levels around 900–850 mb and another minimum around 250 mb. Douglas (1992a) noted that the onset vortex was not restricted to the lower troposphere. By making the lower maximum in the heating more than the upper maximum (as in Fig. 3a), one can obtain the lower-level low stronger than the upper low, as can be seen in Fig. 16a. Also note in Fig. 17b a weak cold core in the lower levels and a stronger warm core in the upper levels with two maxima, one around 700 mb and the other around 350 mb. This qualitatively agrees with the thermal structure of monsoon depressions noted by several authors, as mentioned in the introduction. Temperature shows a westward inclination with height similar to what was observed by Douglas (1992a). As we have already noted, this mode has a westward phase speed and has a high growth rate. We identify this as the monsoon depression since it shows many of the observed characteristics.

A qualitative explanation for the thermal structure noted in Fig. 17b can be attempted. Latent heating has two maxima in the vertical (at 750 and 350 mb, see Fig. 13b) west of the trough where there is rising motion. To the west of the trough there is advection of warm air (note that at higher levels the mean temperature increase to the north). The heating and advection

of warm air overcompensates for the adiabatic cooling, resulting in net warming west of the trough at two heights since there are two maxima. Since the wave is moving westward, this leads to two centers of warm core in the trough. At lower levels because of the curvature of the zonal wind, the meridional gradient of temperature is weakly negative. Further, cumulus heating is either small or zero. This leads to a cold core trough at the lower levels.

Also from Figs. 17b and 17c it can be noted that there is a negative correlation between vertical velocity ω and temperature, indicating a conversion of eddy available potential energy into eddy kinetic energy.

5. Concluding remarks

In the present article a moist baroclinic instability process is studied for easterly and westerly zonal wind shears, including the effects of cumulus friction, Rayleigh friction, and Newtonian cooling. Regarding the latent heating distribution in the vertical, two profiles are used, one having a single maximum and the other having a double maximum. Dissipative effects and the type and intensity of heating changes the selection of the most unstable wave. For the case of double heating, and when all the dissipative effects are included, the most unstable wave turns out to be the Green mode.

The analysis is extended to the Indian monsoon case using the observed zonal wind and temperature profiles representative of this region. In the case of a double maximum in the heating profile, which represents the monsoon case, the most unstable wave shows the vertical structure similar to that of observed monsoon depressions. Particularly, the temperature shows a westward inclination, as was observed by Douglas (1992). This wave can be identified as the Green mode. Also the temperature shows a cold core in the lower levels and a warm core aloft. This is in qualitative agreement with observations.

There is increasing evidence that the nonmodal form of instability is often very relevant to the cyclogenesis (M. Mak personal communication, 1994). Thus, a nonlinear initial value problem approach (as suggested by one of the reviewers) is ideal for studying the evolution of an individual disturbance such as those studied by Douglas (1992). However, the present study served the purpose of understanding the role of several processes in moist baroclinic instability.

Acknowledgments. We are grateful to Prof. Mankin Mak for going through the manuscript and offering valuable comments. Thanks are due to Dr. Kioshi Hada for critically going through the manuscript. Thanks are also due to Drs. Antonio Divino Moura and Carlos A. Nobre and Antonio O. Manzi for providing facilities to conduct this work and for their interest. Penetrative comments of the official reviewers led to substantial improvement of the manuscript.

APPENDIX

Glossary of Symbols

c	Phase velocity (m s^{-1})
c_p	Specific heat at constant pressure (m^2 s^{-2} K^{-1})
D	Half-channel width (m)
DK_b	Energy dissipation by cummulus friction (m^2 s^{-2})
D_{η_T}	Energy dissipation by Newtonian cooling (m^2 s^{-2})
D_{η_ξ}	Energy dissipation by Rayleigh friction (m^2 s^{-2})
f	Coriolis parameter
G	Generation of perturbation available potential energy by diabatic heating (m^2 s^{-3})
h	Vertical structure of heat source
J	Number of layers in the vertical
k	Zonal wavenumber (m^{-1})
K	Kinetic energy of the perturbation (m^2 s^{-2})
K_b	$(= gM_c)$: variable associated with the mass flux in a cloud (N m^2 s^{-1})
K_d	$[= g(dM_c/dP)]$: variable associated with the variation of mass flux in a cloud (s^{-1})
L	Wavelength (m)
l	$[= (\pi/D)]$
M_c	Vertical mass flux in the cloud (kg m^{-2} s^{-1})
M_{c0}	Vertical mass flux in a model level nearest to the base of cloud
P	Pressure (mb)
P_b	Pressure at the base of the cloud (mb)
P_s	Surface pressure (mb)
P_T	Pressure at the top of model atmosphere (mb)
P_*	Pressure at the top of heating (mb)
$\bar{P}$	Mean available potential energy (m^2 s^{-2})
P'	Perturbation available potential energy (m^2 s^{-2})
$\dot{Q}$	Rate of diabatic heating (m^2 s^{-2})
R	Gas constant
U	Mean zonal wind (m s^{-1})
β	Rossby parameter (m^{-1} s^{-1})
ϵ	Arbitrary parameter related to the intensity of latent heat (km hPa^{-1})
η	Coefficient of Newtonian cooling (s^{-1})
η_ξ	Frictional coefficient (s^{-1})
ν	Function that gives the vertical mass flux
ξ	Vorticity (s^{-1})
σ	Static stability (m^2 s^{-2} mb^{-2})
ϕ	Geopotential (m^2 s^{-2})
ψ	Streamfunction (m^2 s^{-1})
ω	Vertical "P" velocity (mb s^{-1})

REFERENCES

Arakawa, A., and W. H. Shubert, 1974: Interaction of cumulus cloud ensemble with the large-scale environment. *J. Atmos. Sci.*, **31**, 673–701.

——, and S. Moorthi, 1988: Baroclinic instability in vertically discrete systems. *J. Atmos. Sci.*, **45**, 1688–1707.

Aravequia, J. A., 1993: A theoretical study of the Green modes (in Portuguese). M.S. thesis, Instituto Nacional de Pesquisa Espaciais, São José dos Campos, Sao Paulo, Brazil, 79 pp.

Bonatti, J. P., 1987: Finite amplitude evolution of baroclinic waves in the atmosphere and ocean (in Portuguese). Ph.D thesis, Instituto Nacional de Pesquisas Espaciais, São José dos Campos, Sao Paulo, Brazil, 311 pp.

——, and V. B. Rao, 1987: Moist baroclinic instability in the development of North Pacific and South American intermediate-scale disturbances. *J. Atmos. Sci.*, **44,** 2657–2667.

Bretherton, F. P., 1966: Critical layer instability in baroclinic flows. *Quart. J. Roy. Meteor. Soc.*, **92,** 325–334.

Chandrasekhar, S., 1961: *Hydrodynamic and Hydromagnetic Stability.* Clarendon Press, 654 pp.

Daggupaty, S. M., and D. R. Sikka, 1977: On the vorticity budget and vertical velocity distribution associated with the life cycle of a monsoon depression. *J. Atmos. Sci.*, **34,** 773–792.

Douglas, M. W., 1992a: Structure and dynamics of two monsoon depressions. Part I: Observed structure. *Mon. Wea. Rev.*, **120,** 1524–1547.

——, 1992b: Structure and dynamics of two monsoon depressions. Part II: Vorticity and heat budgets. *Mon. Wea. Rev.*, **120,** 1548–1564.

Eady, E. T., 1949: Long waves and cyclone waves. *Tellus,* **1,** 33–52.

Geisler, J. E., 1981: A linear model of the Walker circulation. *J. Atmos. Sci.*, **38,** 1390–1400.

Godbole, R. V., 1977: The composite structure of the monsoon depression. *Tellus,* **29,** 25–40.

Hess, S. L., 1959: *Introduction to Theoretical Meteorology.* Holt, Reinehart and Winston, 362 pp.

Holopainen, E. D., 1961: On the effects of friction in baroclinic waves. *Tellus,* **12,** 363–367.

Krishnamurti, T. N., R. Godbole, C. G. Chang, F. Carr, and J. H. Chow, 1976: Study of monsoon depression (1) synoptic structure. *J. Meteor. Soc. Japan,* **54,** 227–239.

Kuo, Y. H., M. A. Shapiro, and E. G. Donald, 1991: The interaction between baroclinic and diabatic processes in a numerical simulation of a rapidly intensifying extratropical marine cyclone. *Mon. Wea. Rev.*, **119,** 368–384.

Lindzen, R. S., 1993: Baroclinic neutrality and the tropopause. *J. Atmos. Sci.*, **50,** 1148–1151.

——, 1994: The eady problem for a basic state with zero PV gradient but $\beta \neq 0$. *J. Atmos. Sci.*, **51,** 3221–3226.

Lupo, A. R., P. J. Smith, and P. Zwack, 1992: A diagnosis of the explosive development of two extratropical cyclones. *Mon. Wea. Rev.*, **120,** 1490–1523.

Mak, M., 1982: On moist quasi-geostrophic baroclinic instability. *J. Atmos. Sci.*, **39,** 2028–2037.

——, 1994: Cyclogenesis in a conditionally unstable moist baroclinic atmosphere. *Tellus,* **46A,** 14–33.

Mishra, S. K., and P. S. Salvekar, 1980: Role of baroclinic instability in the development of monsoon disturbances. *J. Atmos. Sci.*, **37,** 383–394.

Moorthi, S., and A. Arakawa, 1985: Baroclinic instability with cumulus heating. *J. Atmos. Sci.*, **42,** 2007–2031.

Nitta, T., and K. Masuda, 1981: Observational studies of a monsoon depression developed over the Bay of Bengal during summer Monex. *J. Meteor. Soc. Japan,* **59,** 672–682.

Phillips, N. A., 1954: Energy transformation and meridional circulation associated with simple baroclinic waves in a two-layer quasi-geostrophic model. *Tellus,* **6,** 273–286.

Saha, K., and C. P. Chang, 1983: The baroclinic process of monsoon depressions. *Mon. Wea. Rev.*, **111,** 1506–1514.

Satyamurty, P., 1983: Generation of subsynoptic scale unstable baroclinic waves by surface friction. *J. Atmos. Sci.*, **40,** 2075–2079.

Satyan, V., R. N. Krishnamurty, B. N. Goswani, S. K. Dash, and H. S. S. Sinha, 1980: Monsoon cyclogenesis and large-scale flow patterns over South Asia. *Proc. Indian Acad. Sci.*, **89,** 277–292.

Schneider, E. K., and R. S. Lindzen, 1976: A discussion of the parameterization of momentum exchange by cumulus convection. *J. Geophys. Res.*, **81,** 3158–3160.

Shukla, J., 1977: Barotropic–baroclinic instability of zonal mean wind during summer monsoon. *Pure Appl. Geophys.*, **115,** 1449–1462.

——, 1978: CISK-barotropic-baroclinic instability and the growth of monsoon depressions. *J. Atmos. Sci.*, **35,** 495–508.

Wang, B., 1990: On the asymmetry of baroclinic instability between easterly and westerly shear. *Tellus,* **42A,** 463–468.

——, A. Barcilon, and L. N. Howard, 1985: Linear dynamics of transient planetary waves in the presence of damping. *J. Atmos. Sci.*, **42,** 1893–1910.

Yamazaki, M., 1969: Large-scale disturbances in the conditionally unstable atmosphere in low latitudes. *Pap. Meteor. Geophys.*, **20,** 289–336.